CFD ICING SIMULATIONS ON A FIXED-WING UAV ENGINE INLET

Lukas Wurst[1,2], Joachim Wallisch[2,3], Richard Hann[2,3]
[1] University of Stuttgart, Institute of Aerodynamics and Gas Dynamics, Stuttgart, Germany
[2] Norwegian University of Science and Technology (NTNU), Department of Engineering Cybernetics, UAV Icing Lab, Trondheim, Norway.
[3] UBIQ Aerospace, Trondheim, Norway

Abstract

Unmanned aerial vehicles (UAVs), or drones, are increasingly used in diverse commercial and military applications. Ensuring their reliability is crucial to prevent endangering mission targets, people, and infrastructure. All-weather capability is essential for UAVs to operate effectively in various conditions. One major risk is atmospheric icing, which can occur when flying through clouds, affecting aerodynamics and performance. While manned aviation has well-established ice protection systems, applying this knowledge to small fixed-wing UAVs remains challenging, leading to significant knowledge gaps. The air intake of UAV engines is a particularly critical and underexplored area, where icing can reduce engine performance, affecting the UAV's endurance and mission success. This study employs numerical simulations using ANSYS FENSAP-ICE to investigate the icing process at the engine air intake of two different UAV models. The results show that icing significantly impacts air mass flow, necessitating a 4.4 $\%$ increase in inlet velocity to maintain adequate flow. Furthermore, three-dimensional geometry simulations are essential for accurately considering icing at the engine air intake, as the simulations reveal significant variations in ice accumulation and formation between three-dimensional and two-dimensional simulations. The results can give the UAV operator and the manufacturer an indication of the severity of the ice accretion. From this, countermeasures such as the implementation of an IPS can be derived, or possible optimizations in the designs can be identified.

Keywords

unmanned aerial vehicle; atmospheric icing; engine air intake; numerical simulations

NOMENCLATURE

Symbols

$\dot{m}$	mass flow	[kg/s]
ρ	density	[kg/m^3]
v	velocity	[m/s]
A	cross-section	[m^2]
p	pressure	[Pa]

Abbreviations

CFD	computational fluid dynamics
EASA	European Aviation Safety Agency
FAA	Federal Aviation Administration
LWC	liquid water content
MVD	median volume diameter
UAV	unmanned aerial vehicle
UAM	urban air mobility

1. INTRODUCTION

Due to the continuous development and technical progress of drones, their applications and popularity are increasing [1]. While many associate drones with military operations due to news reports from war zones, their uses are vast, ranging from aerial photography and package delivery to search and rescue missions, scientific exploration, and surveillance [1]. Another ongoing topic is the development of air taxis without onboard pilots to reduce city center traffic congestion and improve environmental friendliness, as depicted in NASA's concept of urban air mobility (UAM) environments [2]. Package delivery by drone is also gaining importance, aiming for quick doorstep delivery after online orders.

The variety in unmanned aerial vehicle (UAV) designs is wide, from small quadcopters to military drones larger than airliners. Ensuring high reliability and safety is crucial, especially for operations above populated areas or in remote locations with harsh weather conditions, including atmospheric in-flight icing in cold regions [1]. In-flight icing occurs when supercooled water droplets in the cloud are hitting the surface of the aircraft and freeze [1]. Since in stationary flight, an aircraft relies on lift generated by its wings or rotors, the propulsion system of the aircraft is engineered to counteract the aerodynamic drag and to propel the aircraft [3]. The accumulation of ice on the aircraft's airframe has a detrimental effect on all of these elements. The amount of performance loss experienced by a UAV airfoil in different meteorological icing conditions depends on the shape and thickness of the ice formed and how much it influences the aerodynamics [4]. A study by Fajt et al. [5] using numerical simulations found that the lift can be reduced by 35%, the stall angle can be reduced by 33%, and drag can increase by up to 160% in the worst case.

doi: 10.25967/610455

Besides the degradation of aerodynamic properties caused by ice accretion, a change in surface roughness takes place, resulting in increased drag and a reduction of lift. This happens even without any alteration to the shape of the airfoil as a result of the ice accretion. The increased roughness can also lead to a transition of the flow or even flow separation, which also affects the aerodynamics of the aircraft or UAV [6].

The previously stated implications are applicable not only to a standard airfoil, but also to an engine inlet. Although the decrease in lift may be of lesser significance, ice build-up can obstruct the inlet cross-section and result in reduced performance [7]. This is due to the reduction in cross-section, which reduces the flow of air into the engine. Additionally, the detachment of ice from the leading edge of the air intake may cause harm to the engine blades or engine itself [8, 9].

UAVs exhibit increased vulnerability to the accumulation of ice due to their smaller air inlets and overall size compared to those of conventional aircraft [10]. Despite this disparity in size, both types of aircraft experience similar levels of ice accumulation. This leads to a higher proportion of ice relative to the total size or mass of the UAV, increasing the likelihood of damage. Additionally, according to the study by Zhao et al. [11], UAVs typically have a limited energy storage capacity, which makes it challenging to power an ice protection system. Energy distribution must always be carefully balanced to ensure it meets the mission objectives and maximizes aircraft endurance.

To identify these safety and reliability risks early during development, simulations are essential, providing cost-effective ways to take countermeasures and reduce reliance on expensive wind tunnel tests [12]. However, the complexity of physical phenomena involved presents challenges, and a balance must be struck between prediction accuracy and computation time. Therefore, further research is necessary to better understand simulation methods and the behavior of atmospheric in-flight icing on UAVs, enabling accurate and efficient representation of reality for reliable predictions. This will unlock the full potential of UAVs, expanding their applications while ensuring necessary safety and reliability.

The aim of this work is to close the knowledge gap on icing at the engine inlet of UAVs. This is necessary because icing in this area of the UAV represents a potential risk for flights under icing conditions. For this purpose, numerical simulations are used to assess the magnitude of the degradation, as well as the severity of different conditions, and to provide a foundation for further work.

2. METHODS

In this work, the icing behavior of two different UAV models is investigated using numerical simulations of engine inlet icing, aiming to find the most critical conditions and quantify the performance impact. First, the simulation settings are validated using the results from the work of Yugulis et al. [7] and subsequently, the icing behavior of the air intake of the unmanned aircraft system PX-31 Falk of the company Maritime Robotics is investigated.

2.1. Numerical method

The simulations in this study were conducted using the software FENSAP-ICE (version 2022 R2) by ANSYS to perform simulations for the ice accretion process. This commercial state-of-the-art computational fluid dynamics (CFD) solver is a software package that consists of three linked modules, which in combination can map the complete icing process. These modules are FENSAP, DROP3D, and ICE3D and their interactions can be seen in Figure 1. FENSAP calculates and provides the airflow solution [13, 14]. This solution is subsequently utilized by DROP3D to determine the water distribution on the airfoil's surface [13, 15]. Finally, ICE3D employs the results obtained from DROP3D, in addition to shear stress and heat flux distribution obtained by FENSAP, to determine the ice accretion [16].

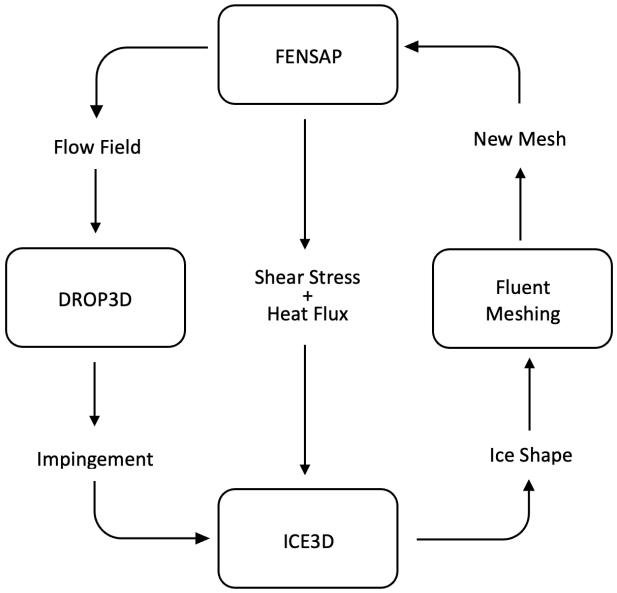

FIG 1. Interaction during the simulation process of the FENSAP-ICE modules.

There is also the possibility of using a multi-shot approach for ice accretion simulations. This implies that the total duration of the icing is split up into smaller intervals. After each interval, the grid around the geometry is updated by automatic remeshing to fit the new ice shape. This remeshing step is performed using ANSYS Fluent meshing [17]. The same grid settings are used for remeshing as for the original grid.

The k-ω-SST model was used as the turbulence model for all simulations, as it provided good results in previous simulations. According to ANSYS [13], this model effectively combines the favorable outcomes of the k-ϵ model in free-flow and the favorable outcomes of the k-ω model near the wall. This is made possible through the utilization of a step function between the k-ϵ and the k-ω model. The k-ϵ transport equations are employed outside the boundary layer and the k-ω transport equations are employed within the boundary layer. All other settings for the simulation can be found in Table 1.

2.2. The validation model

All initial grids used for the simulation were created using the CFD preprocessor Pointwise (version 18.6 R4). First of all,

Parameter	Setting
Transition model	Intermittency model
Gravity	Included with 9.81 m/s^2
Steady / unsteady	multiple steady simulations
Artificial viscosity	Streamline upwind
Droplet distribution	Monidisperse
Ice density	917 kg/m^3

TAB 1. General settings for the simulations.

Parameter	Value
Angle of attack	0 °
Air temperature	22 F (267.59 K)
Ambient pressure	101325 Pa
Droplet MVD	15 μm
Droplet distribution	Monodisperse
Liquid water content	0.7 g/m^3
Wind tunnel geometry (L/W/H)	20 ft / 9 ft / 6 ft

TAB 2. Data and boundary conditions for the simulations of the validation model.

a 2.5D grid was created for the validation model, in which the farfield has the geometry of a wind tunnel, like in the reference [7]. Here, the entire mesh was created from unstructured tetrahedral elements, with a finer grid resolution near the engine air intake with a target value for $y^+ \leq 1$ for the first grid point, which should deliver good results according to Schwarze [18]. The mesh in the area of the air intake can be seen in Figure 2.

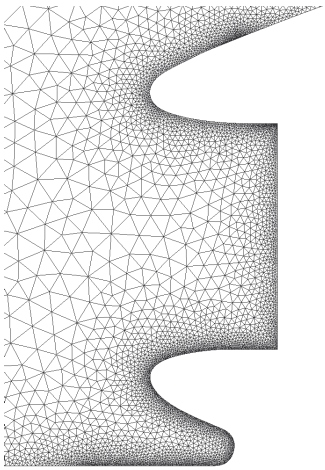

FIG 2. Closeup of the engine inlet of the validation model.

For the validation of the settings, the results from the work of Yugulis et al. [7] were used. In this work, the icing behavior at the engine air inlet of a UAV similar to a General Atomics MQ9 was investigated. This investigation was carried out using numerical and experimental methods and the results were then compared. Only a few parameters are given in the work of Yugulis et al. [7]. Hence, many parameters for the simulations in this paper had to be estimated or found by comparison with figures in the original paper. For the validation simulation, a constant air mass flow of 3.49 kg/s was specified in the engine inlet, as well as an air speed of 87 m/s in the wind tunnel. At the end of the wind tunnel, the air was expanded to the ambient pressure. All other surfaces were defined as walls. The total icing time is 150 s, divided equally into six shots. The properties of the droplets in the air can be defined by the median volume diameter (MVD) as well as the liquid water content (LWC). The MVD classifies the size of the droplet and the LWC the amount of liquid water in the air, which has the unit mass per volume. All other settings and boundary conditions are shown in Table 2.

2.3. Various icing conditions

In order to investigate the different icing conditions, a grid was created as a 2.5D model analogous to the validation model, representing the cross-section in the symmetry plane of the UAV. The PX-31 itself has a length of 1.2 m and instead of a wind tunnel environment, a cylinder with a diameter of 20 times the length of the UAV was chosen as the farfield. A closeup view of the area of the engine inlet of this grid can be seen in Figure 3. This air inlet was designed for this investigation and is inspired by a previous market analysis of other small fixed-wing UAVs.

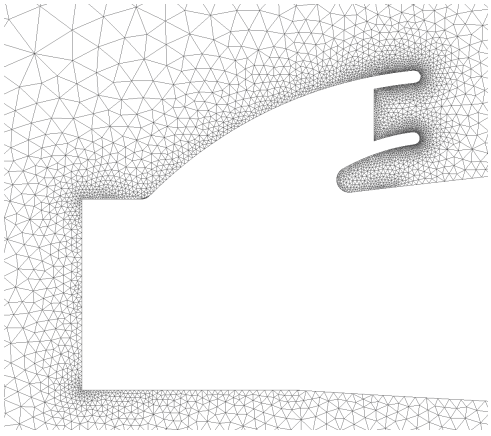

FIG 3. Grid in the area of the engine inlet of the PX-31 Falk.

For the subsequent investigation of the 2.5D model of the PX-31 Falk, various icing conditions were chosen, which were guided by Appendix C [19] of the FAA's Aircraft Certification Regulations, which correspond to those specified by the EASA. For the investigation in this work, three different temperatures at an MVD of 20 μm were chosen from the envelope for continuous maximum icing conditions. This MVD was selected because, according to Fajt et al. [5], it has proven to be particularly unfavorable for typical UAV flight conditions. The temperatures -2 °C, -5 °C, and -10 °C were used because they are typical for the accumulation of glaze, mixed, and rime ice on UAVs [20, 21], whereby all three types of icing can be mapped. Furthermore, to avoid being restricted to a single value of the MVD, simulations were conducted at a temperature of -5 °C for MVDs of 15 μm and 40 μm as well. The various temperatures with the corresponding icing regimes as well as the LWC resulting from Appendix C are summarized in Table 3.

Appendix C also specifies the standard distance for the horizontal extent of these icing conditions of 17.4 nautical miles (32,225 m). By dividing this distance with the cruise speed of the PX-31 Falk of 25 m/s, an exposure time of 1289 s is calculated. This value is used as the icing time in the simulations, which are divided into a total of 10 shots. This number of shots results from a previous shot study.

Regime	Temperature [°C]	LWC [g/m^3]	MVD [µm]
Rime	−10	0.42	20
Mixed	−5	0.7	15
Mixed	−5	0.53	20
Mixed	−5	0.13	40
Glaze	−2	0.59	20

TAB 3. Icing conditions for the simulations.

An icing time of 29 s was selected for the first and 140 s for each of the remaining 9 shots. The reason for simulating with a shorter first shot is related to the surface roughness implementation. Typically, the surface roughness of ice is calculated in ICE3D and used for the subsequent flow simulation in FENSAP. However, an initial roughness height must be specified for the first shot to have a non-zero heat flux at the surface. To reduce the influence of the choice for the initial roughness value, the first step duration is set to a shorter period [22].

In addition, a monodisperse droplet distribution was chosen for all simulations as well as a constant air mass flow into the engine air intake of 80.2 g/s.

To evaluate and assess the findings, three parameters were established. These are the pressure and the velocity at the engine inlet, as well as the ice shape itself resulting from the respective simulation. Due to the narrowed cross-section of the air intake caused by icing, the velocity should increase in order to maintain the air mass flow. Furthermore, the pressure should be reduced as an effect of this.

2.4. Investigating 3D influences

The second grid of the PX-31 is a 3D grid to investigate a possible influence of 3D effects on the simulation. To keep the number of elements low, the wings of the 3D model were shortened slightly, as shown in Figure 4. The UAV has a length of 1.2 m and a remaining wingspan of 0.74 m. A cylinder with a diameter of 20 times the length of the UAV was chosen as the farfield. The cylinder has a width of 2.4 m, which is slightly more than three times the wingspan. This width represented a sufficient compromise between the computational requirements and the accuracy of the results.

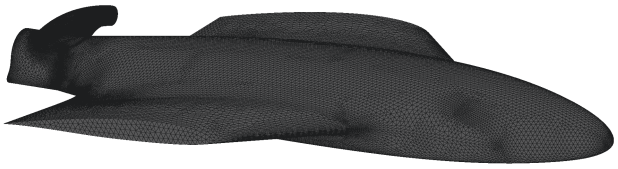

FIG 4. Geometry and Mesh of the PX-31 Falk used for the 3D simulation.

A temperature of −5 °C and an MVD of 20 µm were chosen as boundary conditions for this simulation. The icing time and all other settings are identical to those from the investigation in 2D in order to achieve good comparability. However, the simulation differed in that a single-shot instead of a multi-shot approach was selected. This decision was based on the objective of investigating the distribution of ice accumulation along the leading edge of the engine inlet, rather than investigating the ice shape itself in this area as well as its influence. As a result, the icing duration for this single-shot was set to the full duration of 1289 s.

An additional distinction is that the area of the inlet in this model is slightly smaller than that of the model with the 2D curve. This is due to the fact that the two models have a different extension in the z-direction. Therefore, using equation (1) a new air mass flow of 73.7 g/s was determined.

$$\dot{m} = \rho \cdot v \cdot A = const. \tag{1}$$

The airspeed of 25 m/s and the air density of 1.311 kg/m^3 were kept constant. This new air mass flow was then specified as a parameter for the simulation, same as in the previous simulations.

3. RESULTS

In this chapter, all results and findings from the simulations carried out in this paper are presented. First, the result of the validation model is presented to confirm the numerical method used. Then, the results of the PX-31 Falk for different icing conditions are presented. Finally, the results of the simulation with the complete fuselage of the PX-31 are shown and compared with the previous results in order to present the influence of 3D effects.

3.1. Validation

To verify the numerical method used for the simulations in this study, the model that was investigated in the work of Yugulis et al. [7] was reproduced as a 2D cross-section and then compared with its results. However, since only graphical results are available in the paper, only these could be used for the evaluation. For this purpose, a contour plot of the flow field at the symmetry plane and the ice shape at this cross-section are used for this validation.

3.1.1. Evaluation of the flow field

The first step in this simulation was to match the flow field from the reference case. For this purpose, no icing was taken into account and the simulation was carried out in the clean state. Since the contour plot, which can be seen in Figure 14 in the work of Yugulis et al. [7], is only given with the specification of a dimensionless velocity, the aim was to match this distribution as accurately as possible.
Figure 5 shows the resulting velocity plot from the simulation carried out with this model for validation.

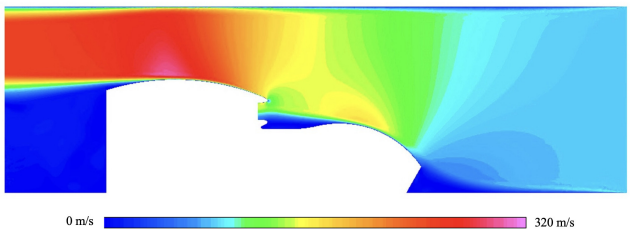

FIG 5. Velocity distribution resulting from the simulation at a velocity of 87 m/s.

As can be seen in a direct comparison of the velocity distributions, a noticeable deviation in the velocity magnitude between the air inlet and upper wind tunnel wall

is observed. The airspeed in this simulation is not only significantly higher, it also occurs over a larger area rather than just locally. In the work of Yugulis et al. [7], the velocity was predominantly high only above the maximum curvature of the geometry. Additionally, differences in the velocity distribution are also observed in the region below the leading edge of the engine air inlets and at the tip of the UAV. The reference plot only shows narrow streamlines with low velocity at these points, while the performed simulation presents a more extensive region within this velocity range. However, it should be noted that the observed differences could be attributed to 3D effects that were not fully accounted for in this simulation. In the three-dimensional model utilized by Yugulis et al., the flow near the leading edge of the model can escape over the sides around the geometry, resulting in the absence of stagnation points at such undercuts. Conversely, in the present two-dimensional cross-sectional simulation, the air can only exit against the direction of flow, leading to its accumulation in such regions. Furthermore, the velocity in the region ahead of the drone at the wind tunnel entrance is observed to be lower than the reference. However, this could imply a shifted velocity spectrum due to the notably higher airspeed present above the intake. A region that is matched in a good approximation is the upper part of the air inlet, where the velocity is in a medium range both in the simulation result and in the reference. The area above the slight curvature in the front of the UAV also has a very similar velocity distribution, although this is slightly larger in the given plot.

3.1.2. Evaluation of the ice accretion and the ice shapes

Since ice only accumulated on the top leading edge of the air inlet, this resulting ice shape is now compared with the one of the validation case by Yugulis et al.. These two resulting shapes are superimposed in Figure 6.

Upon a direct comparison of the ice shapes resulting from the numerical simulation with the corresponding validation case, a high degree of similarity is observed. The ice shapes at the leading edge of the air inlet are highly comparable in terms of their size, shape, and position, with only a minimal discrepancy detected in the ice horn, which is slightly less noticeable in the simulation. Furthermore, a slight difference is also observed in the bottom area, where the icing limit is further downstream in the validation case.

This similarity provides compelling evidence of the accuracy and precision of the numerical simulation employed to predict ice formation in this case. The agreement between the ice shapes in the simulation and validation cases suggests that the simulation model, as well as the chosen settings and physical phenomena, are correctly reproduced, and the results obtained from the simulation are reliable.

By observing the ice shapes resulting of the simulation, it further can be seen that, in contrast to the reference case, no ice has accumulated at the lower side of the inlet. This could be explained by considering the low velocity in this area of the flow field. Since the velocity is so low, no droplets are guided to this leading edge via the streamlines. This assumption can be confirmed by looking at the droplet collection efficiency in this area. In contrast to the upper edge, no droplets are collected by the geometry on the lower edge, which in turn prevents ice accumulation. This

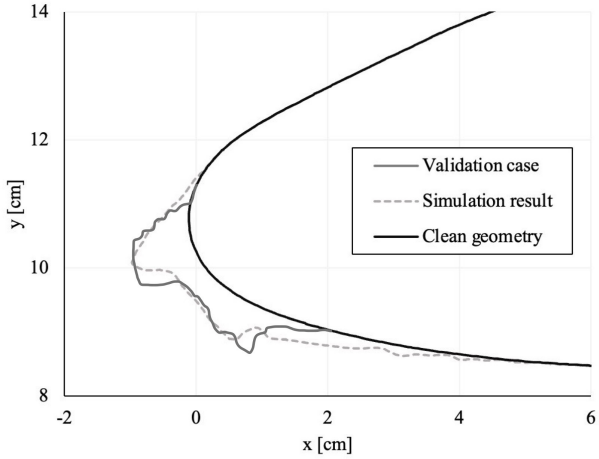

FIG 6. Superposition of the ice shape at the leading edge resulting from the simulation with the ice shape of the reference paper.

is probably due to the 2D simulation carried out here, where three-dimensional effects cannot be reproduced.

3.2. Various icing conditions

This section presents the results for the icing conditions listed in Table 3. Since in these simulations, as in the validation, ice only accumulated on the upper side of the air intake, only graphs of the top of the inlets are shown in this section.

3.2.1. Various temperatures

First of all, the results of the simulations at different temperatures are presented. Figure 7 shows all the resulting ice shapes superimposed. It can be seen that at the lowest temperature of -2 °C the largest ice shape accumulates. This is extended forward in the flight direction and becomes wider. The smallest ice shape results for a temperature of -10 °C. This is shorter and, as expected for the temperature, more streamlined. The size of the ice thickness at -5 °C is in between the two mentioned before, but it is closer to that of -2 °C. In addition, this ice shape also becomes slightly wider towards the top.

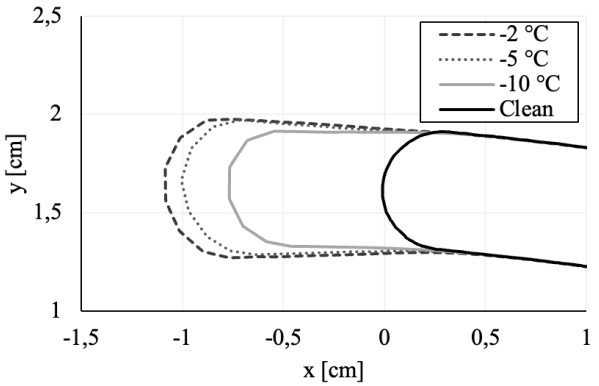

FIG 7. Resulting ice shape at the upper leading edge of the engine inlet of the PX-31 at different temperatures: MVD: 20 μm, airspeed: 25 m/s, icing duration: 1289 s.

The influence of the amount of ice accumulation is also reflected in the relative changes in velocity at the engine inlet shown in Table 4. The largest ice layer at -2 °C shows an increase in velocity of 4.4 %, while the smallest ice shape at -10 °C only shows an increase in velocity of 1.6 %. The relative change in pressure, however, is quite similar, with a 2.4 % decrease at -2 °C and -5 °C and a 2.3 % decrease at -10 °C.

Temperature [°C]	Δp [%]	Δv [%]
-2	-2.4	4.4
-5	-2.4	3.5
-10	-2.3	1.6

TAB 4. Resulting change in pressure and velocity in the inlet from the simulations for different temperatures.

The fact that the three ice accumulations have a different size could be due to the respective LWC. As can be seen in Table 3, the LWC decreases with decreasing temperature, resulting in a reduced water content in the flow that can freeze and accumulate on the surface. Since the icing time is identical in all simulations, this could also result in the different sizes of the ice shapes.

A further explanation for the similar shape of the ice can be found by analyzing the freezing fraction for the three temperatures. The freezing fraction is a non-dimensional parameter used in ice-accretion studies which is defined by the heat-balance analysis of Messinger. This value ranges from 0 (no ice) to 1 (immediate freezing on impact) and has been shown to play an important role in determining the physical appearance of the accreted ice [23, 24]. Here, at -10 °C, the freezing fraction is 0.47, and at -2 °C and -5 °C it is almost 0. This indicates that glaze ice accumulates at all three temperatures, which also fits the three ice shapes. This unusual behavior, especially at -10 °C, could be due to various causes such as the missing prism layers, an insufficient number of grid points, or possibly because 3D effects were neglected in the simulation.

3.2.2. Various MVDs

Figure 8 shows the overlaid ice shapes from the simulations with a variation of the MVD. All simulations were carried out at a temperature of -5 °C. The largest ice accumulation can be seen at an MVD of 15 µm. This ice shape extends narrowly forward in the flight direction. The ice shape from the simulation with an MVD of 20 µm is somewhat shorter, but becomes wider towards its tip. The ice layer at an MVD of 40 µm is barely visible in the figure since it is minimal and is directly on the leading edge.

The largest change in inlet velocity is present for the thickest ice layer at an MVD of 15 µm with an increase of 3.6 %. With an increase of 3.5 %, the ice shape is of the same order of magnitude at an MVD of 20 µm. Even with the only slight ice accumulation at an MVD of 40 µm, an increase in the inlet velocity of 3.0 % and a pressure reduction of 2.3 % can be measured. For the other two MVDs, there is a reduction in pressure of 2.4 %. The relative changes in pressure and velocity across the inlet of the different MVDs are also listed in Table 5.

Similar to the results at different temperatures, the size of the ice shapes correlates to the LWC. This is because the lowest MVD has the highest LWC, which in turn results in a thicker ice shape. At an MVD of 40 µm, the LWC is so low that only a minimal ice layer spreads over the surface.

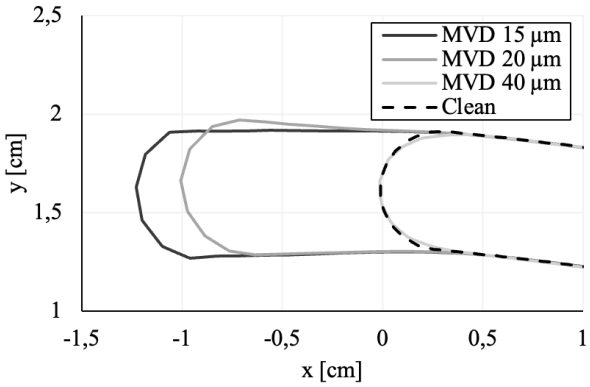

FIG 8. Resulting ice shape at the upper leading edge of the engine inlet of the PX-31 at a temperature of -5 °C and various MVDs: airspeed: 25 m/s, icing duration: 1289 s.

MVD [µm]	Δp [%]	Δv [%]
15	-2.4	3.6
20	-2.4	3.5
40	-2.3	3.0

TAB 5. Resulting change in pressure and velocity in the inlet from the simulations for different MVDs.

3.3. Influence of 3D effects on ice accretion

This section will look into the potential impact of three-dimensional effects. The reason for this investigation comes from the fact that the validation case from the reference paper [7] employed a three-dimensional model, wherein ice accumulated on both the top and bottom of the air inlet. However, when efforts were made to align these outcomes with simulations of a two-dimensional cross-section, ice formation only occurred on the upper side. As similar results were observed in the investigation of the PX-31 Falk using as well a two-dimensional cross-section, this chapter will look into the potential occurrence of this effect in the three-dimensional model of the PX-31. However, the aim here is not to exactly reproduce the ice shapes already presented, but to investigate these three-dimensional effects with the aid of a single-shot simulation. The cross-section shown in Figure 9 is exactly at the symmetry plane of the 3D grid of the PX-31. The selection of this particular cross-section is due to the fact that all other investigations within this study were conducted using the same cross-section, which gives the best comparability of this investigation. As can be observed, an ice shape is formed on this model both on the bottom and on the top side of the engine air inlet.

Upon analyzing the flow field, it is observed that the velocity within the region beneath the engine inlet is no longer in proximity to zero. Although the velocity within this area remains lower than observed in other regions around the UAV, there is no stagnation of air. As such, the flow can exit to the left and right of the geometry beneath the engine inlet and continue to propagate. A noticeable wake zone of the flow can be seen behind the canopy of the inlet.

The modified flow field resulting from the use of the three-dimensional mapping of the geometry has yielded a new distribution of droplet collection efficiency across the sur-

face of the engine inlet. Droplets now hit and collect on the lower part of the leading edge of the inlet, which is a prerequisite for subsequent ice accretion.

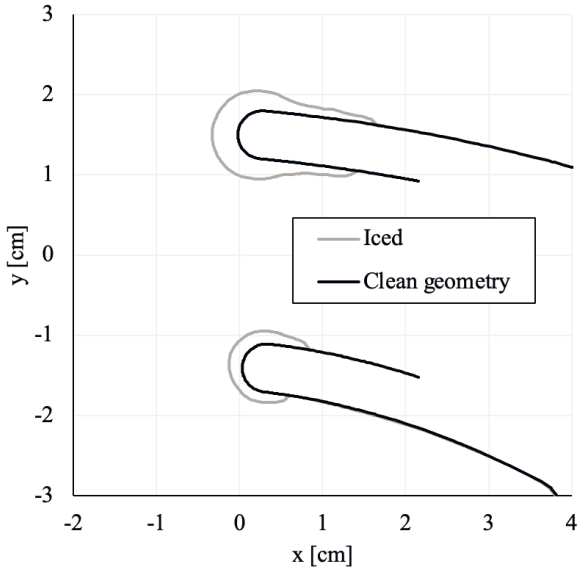

FIG 9. Ice shape of the complete 3D model of the PX-31, cut at the symmetry plane. Icing conditions: airspeed: 25 m/s, ambient temperature: −5 °C, MVD: 20 µm, LWC: 0.53 g/m^3, icing duration: 1289 s.

Figure 10 shows an overlay of the ice accumulation of the 3D geometry and the 2D cross-section resulting from the simulation. Since the simulation of the 3D geometry was carried out as a single shot, the result of the 5 shot simulation was chosen for comparison. The overlay of the two simulations shows a noticeable deviation in the ice accumulations. The ice shape resulting from the 2D simulation is narrower and extends further in the direction of flight. Furthermore, it is apparent that the ice shape accumulating on the 3D geometry is more evenly distributed across the leading edge of the inlet and extends further towards the back. Additionally, there is a larger narrowing of the cross-section in comparison to the 2D result.

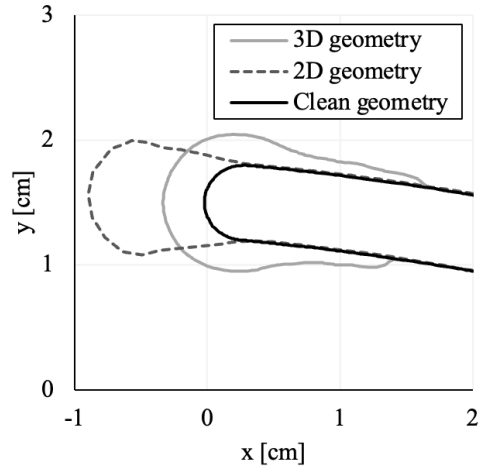

FIG 10. Superposition of the ice shapes resulting from the simulations of the 3D geometry and the 2D cross-section with 5 shots. Icing conditions: airspeed: 25 m/s, ambient temperature. −5 °C, MVD: 20 µm, LWC: 0.53 g/m^3, icing duration: 1289 s.

As demonstrated in the investigation shown here, the unavailability of ice accretion on the lower surface of the engine inlet during the simulation of a two-dimensional cross-sectional area is attributed to the inability of accounting for three-dimensional effects.

Moreover, it was discovered that the ice shape and the areas of ice accumulation exhibited noticeable differences between the simulation of the 3D geometry and the two-dimensional cross-section. However, this could also be due to the difference between the single-shot simulation carried out here and the multi-shot simulation which was set as the reference. Thus, investigating the icing behavior of engine air intakes utilizing 3D geometries could prove useful in accurately depicting the influence.

4. DISCUSSION

The deployment and utilization of UAVs can be greatly affected and limited by the accretion of ice. To mitigate this hazard, it is crucial to identify the susceptible and critical regions on the UAV and take measures to protect them from icing. However, to accomplish this objective, it is necessary to gain a better understanding of this phenomenon, especially since research on icing at smaller UAV scales is limited. First and foremost, CFD simulations offer the possibility to deliver results with less effort and quicker compared to tests in an icing wind tunnel. Nevertheless, these results must undergo experimental studies for validation in subsequent stages of development and investigation.

In this work, the focus was on the accumulation of ice in the area of the air intake on the engine. The aim is to gain a better understanding of the icing phenomena in this region and to investigate the possible influences of ice formation on the engine in general. First of all, an engine inlet typical for the size class was designed for the UAV which was investigated, the PX-31 Falk. Subsequently, for the purpose of investigating the icing behavior, a total of five different icing conditions were analysed with the help of the CFD tool FENSAP-ICE. Furthermore, an examination was conducted to assess the impact of disregarding 3D effects in the simulation of two-dimensional cross-sections.

4.1. Ice accretion and its impact

The parameter study carried out in this work aimed to investigate the icing of the engine inlet of the PX-31 Falk under various icing conditions. Three different temperatures and three different MVDs were investigated.

The largest ice shape occurs for the highest temperature and the smallest ice shape for the lowest temperature. This behavior can be explained by the LWC, since the warmer the temperature, the higher the LWC at a constant MVD. As a consequence, the larger ice accumulation results from this higher water content in the air that impinges on the leading edge.

In the results, summarized in Table 4 and 5, it can be seen that almost the same pressure change of 2.3 % or 2.4 % respectively occurred throughout the entire study.

The velocity change in the inlet shows a larger variation. With a decreasing temperature the influence on the velocity becomes smaller. The same trend can also be seen with

an increase in MVD where the velocity change becomes smaller the higher the MVD is. This is likely related to size of ice shape, since the bigger ice shapes (higher LWC) resulted in a larger velocity changes.

4.2. Influence of neglecting 3D effects

During the validation of the numerical simulation, it was observed that there was no formation of ice on the lower side of the engine inlets, which was consistent with the results of the simulations of the PX-31. Further analysis of the flow field and droplet collection efficiency suggested that this phenomenon may be attributed to the accumulation of air in the undercut region below the air inlet. The two-dimensional cross-section employed in the simulation was extruded in the z-direction, leading to the formation of a three-dimensional grid. Nonetheless, this approach does not represent the actual 3D geometry of the system since it considers only a single cross-section. As a result, the flow cannot escape to the sides and continue to circulate around the surface as it would in a true 3D geometry. Instead, it accumulates, leading to a significant reduction in flow velocity. In order to validate this hypothesis, the 3D model was trimmed at the wings and then meshed and simulated.

The findings presented in chapter 3.3 demonstrate that a distinct layer of ice is now forming on the lower side of the engine inlet. Additionally, an analysis of the flow field reveals that the flow can escape from the undercut and continue to stream around the geometry to both sides. This is further supported by the droplet collection efficiency, which indicates that droplets are now being collected from the lower edge, which is necessary for subsequent ice accumulation.

Noticeable deviations can be seen between the ice shapes of the 2D and the 3D simulation. It can be seen that the ice shape on the 3D geometry is spread more evenly across the leading edge of the engine inlet. In addition, it is thicker compared to the result of the two-dimensional cross-section, which is probably due to the different number of shots.

Another aspect related to the expanded width of the ice shape observed in the three-dimensional geometry is the narrowing of the inlet cross-section on all sides, thereby enhancing its impact. Thus, by analyzing the inlet cross-section, a better evaluation can possibly be made about the influence of the icing than about the evaluation of the pressure and the speed at the inlet. These two factors, especially the pressure, only have a limited informative value, as the results have shown.

These results show that 3D simulations are essential to correctly simulate and map ice deposition at an engine inlet. In contrast, 2D simulations possess limited utility and are only suitable for assessing the influence of diverse icing conditions.

4.3. Uncertainties

This study is subject to uncertainties which must be considered when assessing the outcomes. Firstly, there is little published data and research on the investigation of the icing at the engine inlet of UAVs that could serve as a foundation for validating the numerical simulation or for later comparisons of the results. Secondly, the lack of boundary conditions, such as airspeed or the total duration of icing, in the work of Yugulis et al. [7], and the subsequent need to estimate them, introduces a degree of uncertainty in the validation process. This can be seen, among other things, in the differences in the plot of the velocity distribution.

An additional potential source of error in this study relates to the quality of the grids employed to investigate the PX-31 Falk. Notably, due to limited computational resources and some technical difficulties, the implementation of prism layers along the surface was intentionally waived. Having a mesh with prism layers would have increased both the number of elements within the model and the computational time required by a considerable degree. Moreover, the creation of such layers was kept to a limited extent by the noticeable deflections and edges present on the inlet, which caused the elements to intersect and thereby stop the layering process after a few layers. The impact of the grid is also apparent in the grid-dependence study. The results suggest that convergence has not yet been attained and that more cells or another cell type is required. The shot study carried out with the chosen grid also did not lead to a clear result, and the choice to carry out the following simulations with 10 shots was rather due to the resulting ice shape. However, these two issues are in itself linked to the previous constraint of limited computational resources, as well as the restricted processing time available within the scope of this study.

Furthermore, it was noticed that the pressure remains almost constant over the various icing conditions. Also in the previous shot study, the velocity at the inlet showed a linear dependence on the number of shots rather than on the icing conditions themselves. This behavior of the two parameters evaluated could also indicate that they are not fully suitable for evaluation. Moreover, it would probably be more realistic to specify a constant pressure at the inlet instead of a fixed air mass flow. However, this was not possible in this study due to problems with the software, as these simulations did not result in converging mass flows and therefore represented an uncertainty.

The investigation of 3D effects has revealed their significant impact on the resulting outcomes. Not only do the ice formation and areas of accumulation vary, but they may also affect the pressure and velocity values within the inlet. The assessment and evaluation in this study were based on the continuity equation 1. Thus, the expectation was that if the mass airflow remains constant, the icing will decrease the cross-sectional area of the inlet, causing a subsequent increase in velocity to maintain mass flow. Consequently, the rise in velocity decreases the pressure there. This assumption was reflected in the results, although the simulations only considered the icing on the top of the inlet. In contrast, the simulation with the three-dimensional model showed an ice accretion around the entire inlet edge, reducing the cross-sectional area by a larger factor than in the two-dimensional cross-sectional simulations. This could potentially indicate that the change in the two assessed parameters are more substantial than determined in this study.

4.4. Future work

The outcomes of this study have demonstrated the considerable impact of distinct grids on the results. Thus, future work could employ a higher grid resolution to increase the accuracy of the results. Additionally, the impact of prism

layers on the results can be investigated to explore how they affect the outcomes.

With the availability of sufficient computing power, this investigation should be extended to include three-dimensional geometries, considering the apparent differences in ice accumulation. Furthermore, additional parameters such as changes in the engine inlet cross-section due to icing could be integrated for evaluation. Moreover, other points on the icing envelope could be investigated, such as the icing of SLDs. These are characterized by a droplet diameter greater than 50 microns and have the potential to lead to a significant loss of performance due to rapid and severe ice accretion. Investigations with different temperatures and LWC ranges could also be carried out to find conditions that produce rime ice.

Additionally, new parameters can also be identified for the evaluation of the results, given that the usability of inlet velocity and pressure could not be confirmed based on the results of this short study.

More knowledge on the air mass flow through the engine inlet would be helpful to perform simulations that duplicate the reality as closely as possible. Hence, it is recommended to put more effort in this investigation.

In further investigations, other effects on the engine could also be considered. Conceivable here would be the effects of the suction of ice fragments through the intake into the engine compartment. Also, icing of the carburetor or even of pipes inside the engine compartment could be investigated. Here it is interesting to see whether icing could possibly have other negative effects, apart from performance losses, and thus possibly damage the engine.

5. SUMMARY

In this work, the icing behavior of the engine air intake of UAVs was investigated. For this purpose, the two-dimensional cross-section of the PX-31 Falk was investigated using CFD simulations at various icing conditions. In addition, the influence of 3D effects on the ice accretion in the area of the air inlet was investigated.

A total of five different icing conditions from Appendix C continuous maximum icing conditions were chosen. These include three temperatures and three different MVDs.The simulation settings used in this work were validated with the help of the results presented in the paper by Yugulis et al. [7]. The simulated ice shapes show good agreement on the upper side of the air intake but no ice accretion on the lower side. This is contrary to the results of Yugulis et al. [7].

The parameter study showed that the pressure change is constant over almost all icing conditions, with a reduction of -2.3 % to -2.4 %. Larger influences can be seen with the velocity at the inlet. Both, decreasing the MVD and increasing the temperature results in lower velocities at the engine inlet. However, this study suggests that pressure and velocity may not be useful parameters. Since all ice shapes have a similar shape but vary in size, this could be connected to the respective LWC. As the temperature decreases, the LWC decreases as well, which leads to a decrease in the water content in the flow. As a result, less water hits the surface, which freezes and can accumulate as ice.

During the simulation for the validation of the simulation settings as well as during the investigations of the parameter study, ice only accumulated on the upper side of the engine inlet. Since the analysis of the flow field showed that the flow velocity on the lower side of the inlet was almost zero, this behavior was verified with the simulation of a 3D geometry of the PX-31 Falk. In this 3D simulation, a layer of ice accumulated on the lower leading edge of the inlet under identical icing conditions. An evaluation of the flow field and the droplet collection efficiency also showed a higher velocity and droplet implement in this area. This behavior of the ice accumulation at the lower edge can thus clearly be attributed to the neglect of 3D effects in the simulation of a two-dimensional cross-section.

As these results show, icing at the leading edge of the engine inlet has a noticeable effect on the UAV. As the air mass flow decreases because of icing, it could be possible that the UAV has a lower endurance during operation and thus possible mission objectives can no longer be achieved. However, it should also be taken into account that the results of this study show a variation, especially when comparing the 2D and 3D results. Therefore, in order to make a concrete statement about the icing at the engine inlet, further simulations in 3D should be carried out in any case to verify these effects and influences.

Contact address:

Lukas Wurst, lukas.wurst@gmx.de
Joachim Wallisch, joachim.wallisch@ntnu.no
Richard Hann, richard.hann@ntnu.no

References

[1] Richard Hann and Tor Arne Johansen. Unsettled Topics in Unmanned Aerial Vehicle Icing EPR2020008. Technical report, 2020. DOI: 10.4271/EPR2020008.

[2] Lillian Gipson. Taking Air Travel to the Streets, or Just Above Them. *NASA*, 2018. https://www.nasa.gov/aero/taking-air-travel-to-the-streets-or-just-above-them. Accessed: 2023-02-06.

[3] András Sóbester and Alexander I J Forrester. *Aircraft Aerodynamic Design*. Wiley, 10 2014. ISBN: 9780470662571. DOI: 10.1002/9781118534748.

[4] M.B. Bragg, A.P. Broeren, and L.A. Blumenthal. Iced-airfoil aerodynamics. *Progress in Aerospace Sciences*, 41(5):323–362, 2005. ISSN: 0376-0421. DOI: https://doi.org/10.1016/j.paerosci.2005.07.001.

[5] Nicolas Fajt, Richard Hann, and Thorsten Lutz. The Influence of Meteorological Conditions on the Icing Performance Penalties on a UAV Airfoil. Conference paper, 2019. DOI: 10.13009/EUCASS2019-240.

[6] M.B. Bragg, A.P. Broeren, and L.A. Blumenthal. Iced-airfoil aerodynamics. *Progress in Aerospace Sciences*, 41(5):323–362, 2005. ISSN: 0376-0421. DOI: https://doi.org/10.1016/j.paerosci.2005.07.001.

[7] Kevin Yugulis, David Chase, and Matthew McCrink. Ice Accretion Analysis for the Development of the Heatcoat Electrothermal Ice Protection System. In *AIAA AVIATION 2020 FORUM*, 2020. ISBN: 9781624105982. DOI: 10.2514/6.2020-2834.

[8] Jeanne G. Mason and Matthew Grzych. The Challenges Identifying Weather Associated with Jet Engine Ice Crystal Icing. In *SAE Technical Papers*. SAE International, 2011. DOI: 10.4271/2011-38-0094.

[9] Jeanne G Mason, J Walter Strapp, and Philip Chow. The Ice Particle Threat to Engines in Flight - AIAA 2006-206. 2006.

[10] Krzysztof Szilder and Stuart McIlwain. In-flight icing of uavs - the influence of reynolds number on the ice accretion process. *SAE Technical Papers*, 10 2011. DOI: 10.4271/2011-01-2572.

[11] Y. Zhao, S. Chang, B. Yang, W. Zhang, and M. Leng. Experimental Study on the Thermal Performance of Loop Heat Pipe for the Aircraft Anti-Icing System. *International Journal of Heat and Mass Transfer*, 111:795–803, 2017. ISSN: 00179310. DOI: 10.1016/j.ijheatmasstransfer.2017.04.009.

[12] Richard Hann. *Atmospheric Ice Accretions, Aerodynamic Icing Penalties, and Ice Protection Systems on Unmanned Aerial Vehicles*. PhD thesis, 2020. ISSN: 1503-8181.

[13] ANSYS Inc. *Ansys Fensap-Ice User Manual, Release 20.1*. 2020.

[14] G. S. Baruzzi, W. G. Habashi, J. G. Guevremont, and M. M. Hafez. A Second Order Finite Element Method for the Solution of the Transonic Euler and Navier-Stokes Equations. *International Journal for Numerical Methods in Fluids*, 20(8-9):671–693, 1995. ISSN: 10970363. DOI: 10.1002/fld.1650200802.

[15] Yves Bourgault, Ziad Boutanios, and Wagdi G. Habashi. Three-Dimensional Eulerian Approach to Droplet Impingement Simulation Using FENSAP-ICE, Part 1: Model, Algorithm, and Validation. *Journal of Aircraft*, 37(1):95–103, 1 2000. ISSN: 0021-8669. DOI: 10.2514/2.2566.

[16] Y. Bourgault, H. Beaugendre, and W. G. Habashi. Development of a Shallow-Water Icing Model in FENSAP-ICE. *Journal of Aircraft*, 37(4):640–646, 7 2000. ISSN: 0021-8669. DOI: 10.2514/2.2646.

[17] Switchenko D. Baruzzi G. Ozcer, I. and J. Chen. Multi-shot icing simulations with automatic re-meshing 2019-01-1956. *SAE Technical Papers*, page 15, 6 2019. DOI: 10.4271/2019-01-1956.

[18] Rüdiger Schwarze. *CFD-Modellierung*. Springer Berlin Heidelberg, 2013. ISBN: 978-3-642-24377-6. DOI: 10.1007/978-3-642-24378-3.

[19] Federal Aviation Administration. Icing Design Envelopes (14 CFR Parts 25 and 29, Appendix C). Technical report, 1964. Accessed: 2023-02-06.

[20] Richard Hann. UAV Icing: Ice Accretion Experiments and Validation. SAE Technical Paper. No. 2019-01-2037. 2019. DOI: 10.4271/2019-01-2037.

[21] Richard Hann, R. Jason Hearst, Lars Roar Sætran, and Tania Bracchi. Experimental and Numerical Icing Penalties of an S826 Airfoil at Low Reynolds Numbers. *Aerospace*, 7(4), 4 2020. ISSN: 22264310. DOI: 10.3390/aerospace7040046.

[22] Nicolas Fajt. *The Influence of Meteorological Conditions on the Icing Performance Penalties on a UAV Airfoil*. Master's thesis, University of Stuttgart and Norwegian University of Science and Technology, 2019.

[23] Bernard L. Messinger. Equilibrium Temperature of an Unheated Icing Surface as a Function of Air Speed. *Journal of the Aeronautical Sciences*, 20(1):29–42, 1 1953. ISSN: 1936-9956. DOI: 10.2514/8.2520.

[24] David N. Anderson and Jen-Ching Tsao. Evaluation and Validation of the Messinger Freezing Fraction - AIAA–2003–1218. 2005.

ACKNOWLEDGMENTS

The authors would like to thank Dr. Thorsten Lutz and the Institute of Aerodynamics and Gas Dynamics at the University of Stuttgart for their support and supervision of this work.

Further thanks go to the company Maritime Robotics for providing the 3D model of the PX-31 Falk, which served as the foundation for this work.